Vegetation Canopy Lidar Studies

Stuart A. Young

Vegetation Canopy Lidar Studies

Stuart A. Young

Abstract

With the planned launch of NASA's Vegetation Canopy Lidar on September 2000, the CSIRO Earth Observation Centre is involved in the development of an airborne system for imaging and measuring the structure of the vegetation biomass over Australia. The Vegetation Structure and Imaging System (VSIS) would produce many useful outcomes. Besides its obvious benefits in the commercial arena for mapping and characterising commercial forests and surveying areas to be crossed by electrical powerlines, telecommunication lines, and gas pipelines for example, it would provide valuable scientific data on the vegetation biomass over Australia. The data would be on a finer scale than those from the satellite instruments and could also be used to develop and check the suitability of algorithms to be used for the interpretation of satellite data acquired over Australia. As a prelude to the development of an airborne instrument, several studies were necessary in order to help decide on the specifications of the airborne system. Among those studies was a series of experiments performed with the Multi-Wavelength Scanning Lidar (MWSL) operated by CSIRO Atmospheric Research, culminating in a field trial at Tanjil Bren in which the lidar was used to acquire data from various trees. This lidar was originally designed for the study of the dispersion of smoke plumes from power stations or similar sources, for the study of clouds at all altitudes, and for the study of aerosol layers ranging from the boundary layer to the stratosphere. As the lidar signal from trees at a distance of about 50 m is many orders of magnitude more than the signal from aerosols at an altitude of 50 km, some modification of the MWSL was required. This paper reports briefly on some aspects of the development of the new equipment and methods needed for the ground-based lidar studies of trees, then details the field trial at Tanjil Bren. Finally, some conclusions and recommendations regarding a dedicated vegetation canopy lidar are presented.

1   Introduction

The accurate measurement of the height, coverage, vegetation canopy structure and biomass of forests is of increasing importance. Such information is needed by forest and land managers, ecologists and governments concerned about controlling the levels of greenhouse gases. While aerial photogrammetry and satellite imagery can provide some useful data, these techniques are unable to provide range-resolved information on the structure of the vegetation canopy. This information is essential to the estimates of forest biomass needed by governments involved in carbon trading and greenhouse gas mitigation.

Over the last few years, active remote sensing techniques have been developed for the measurement of forests. These systems have been based around the lidar (or laser radar) technology in which a short pulse of laser light is directed at the forest target and the reflected light is collected in a telescope, detected, then digitised. The signals give the range and strength of all the targets along the path of the laser beam. By scanning the lidar through the forest canopy, information on its structure can be gained. These vegetation lidars have been operated from both gound and airborne systems (Maclean and Krabill; 1986, Nelson et al., 1984). Nilsson (1996) reported on the influence of the size of the laser footprint on the target in the estimation of tree heights and stand volume. Most of the early vegetation lidars were merely modified laser altimeters, which measure only the range to the targets. The SLICER lidar developed by NASA is a one of a new generation of airborne vegetation lidars that feature large, scanned laser footprints (Means et al., 1999). As the larger pulse encounters many more targets along its path, the resulting signal contains more information and is digitised over its whole useful range. The SLICER instrument has been used for the measurement of the biomass of forests in the USA (Lefsky et al., 1999). There are now

several airborne laser scanning systems with different features, and a review of the existing systems and manufacturers has been made by Baltsavias (1999).

While airborne systems are useful for regional measurements, global measurements of vegetation biomass on a timescale that allows the monitoring of seasonal and other changes is only feasible from satellites. NASA plans to launch its satellite-borne Vegetation Canopy Lidar (VCL) (Bufton and Blair; 1996, Dubayah et al., 1997) in September 2000. This has been developed using the experience gained with the SLICER and other instruments. The Laser Vegetation Imaging Sensor (LVIS) (Blair et al., 1999) is the airborne simulator for the VCL and has been used to acquire data for the testing of the performance of the VCL and for developing and testing of data analysis algorithms.

There has been recent interest in acquiring vegetation canopy data in Australia. The CSIRO Earth Observation Centre (EOC) is involved in the development of an Australian Vegetation Structure and Imaging System (VSIS). Such an instrument would provide the data required by Australian land and forestry managers and ecologists as well as companies involved in the laying of pipelines, and the erection of electricity and communication towers through forested areas. The data would also provide a useful validation for the VCL over Australia and enable the development and testing of the suitability of VCL analysis algorithms for Australian trees.

As part of the preliminary investigations into the design specifications for VSIS, CSIRO Atmospheric Research (CAR) was asked at the VSIS meeting in Canberra in March 1999 to assist in these investigations by performing some experiments with its Multi-Wavelength Scanning Lidar (MWSL). The MWSL was modified during 1999 and some preliminary data on local trees acquired at Aspendale. The studies culminated in a field trial at Tanjil Bren in December 1999. This paper reports on the main aspects of the CAR MWSL studies and concludes with some recommendations on the design of the VSIS.

2   Objectives of the studies

The objectives of the canopy lidar research performed with the CAR MWSL were rather straightforward. They were, simply, to acquire lidar data for Australian trees, and to test the effects of various system configurations on the signals that were measured.

There were two main reasons for collecting the lidar data. Firstly, the data could be used in helping to produce specifications for the VSIS, which would incorporate a dedicated vegetation canopy lidar. Important system parameters that need to be defined include, on the transmitter side, the laser energy, repetition rate, pulse length and beam spread, wavelength and polarisation. Important receiver parameters include dimensions, field of view, the type and performance of the detectors, and the number of detector channels and what they should be used to measure. Multiple detector channels could be used, for example, to study the wavelength dependence of the reflected signal, or fluorescence or polarisation effects. Such signals are related to the form and characteristics of the target (leaf or trunk for example) and to the nature and health of the vegetation (Ludecker, et al., 1999; Chappelle et al., 1984, 1999).

Secondly, the data could be used for the development and testing of the various algorithms needed to analyse the VSIS data. Such algorithms need to be able to detect and describe the vertical distribution of the vegetation targets above the local terrain. This involves the

detection of the terrain boundary and the ranges of all the targets along the beam path. The allowance for the attenuation of the beam and for multiple scattering or reflections also needs to be made and this is not an easy task.

3   Lidar signals from solid targets

Although lidar (or laser radar as it is sometimes known) has been used from the outset for measuring the ranges of solid targets (the moon and satellites, and in military applications), the most common research application during the last four decades has been in the study of the atmosphere and its constituents. There are inherent differences in these applications. In the first, the range information is of primary interest, while in the second both the range and the signal characteristics are of importance. The equations describing the signals are also different as they arise from different processes. In the first application the signal arises from the interaction of the laser pulse with the surface of the target. In the second, the signal measured at any instant by the receiver represents the sum of all photons, reaching the receiver at that time, that have interacted with scatterers inside a volume that is common with the laser pulse boundaries and the field of view of the receiver.

Because the CAR MWSL was being used for the first time to measure signals from solid targets at close range, and because knowledge of the likely strength of the signals was important in choosing a system configuration that would permit the detection of the strong signals without damaging or destroying the sensitive detectors, the equations describing the strength of lidar signals from solid targets were derived, and are presented here. Variations of these equations are also needed in the calibration and analysis of the lidar data.

We begin by considering the irradiance at a plane target oriented normal to the path of the transmitted laser beam and located at a distance r from the laser transmitter (Fig. 1).
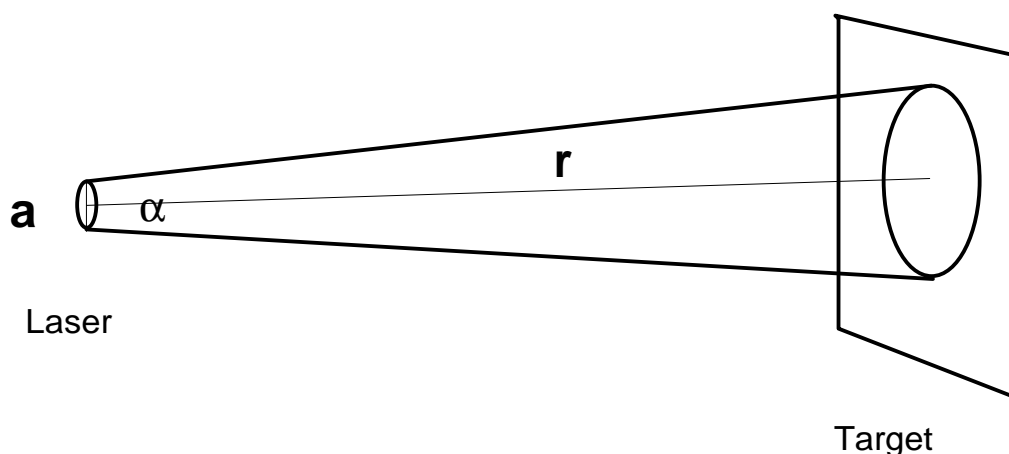
Figure 1. The geometry describing the illumination of the target by the laser beam.

If the full-angle divergence of the laser is α mr, then the area, dS, illuminated at the target by the laser beam is $\pi/4\ (\alpha r)^2$. The solid angle subtended by the beam at the target is $\pi/4\ \alpha^2$. The irradiance at the target is simply

$$E_t\ (W\ m^{-2}) = P_o\ /\ dS = 4P_o\ /\ (\pi\ (a + \alpha r)^2)\ ,$$

where $P_o = P(t)$ is the output power of the laser.

Now, consider the power measured at the receiver due to diffuse reflection from the target. Assume that the target is a Lambertian reflector with reflectance ρ, oriented with its normal at an angle θ to the axis of the receiver. (Note that the axes of the laser transmitter and of the receiver are not perfectly parallel for close range operations.) The focal length of the receiver is f and the receiver field of view is β (Fig. 2).
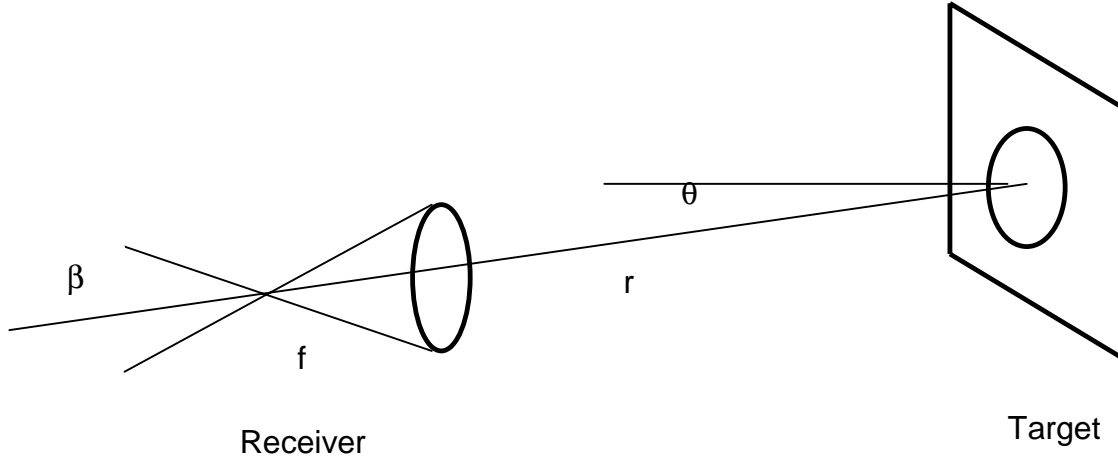
Figure 2. The receiver- target geometry.

The irradiance of the diffusely-reflected radiation at the receiver aperture is

$$E_r\,(\text{W m}^{-2}) = \rho P(t)\cos\theta\,/\,\pi r^2.$$

Now, as the field of view of the receiver is very much greater than the divergence of the laser, the image of the laser spot on the target falls completely inside the receiver field limiting aperture. Therefore, the total receiver power is $E_r A_r$ (W), where A_r is the active area of the receiver. The voltage measured at the detector output is then

$$V_d(t) = \eta_o \tau_{ND}\, S_\lambda R_L A_r \rho P(t)\cos\theta\,/\,\pi r^2,$$

where
η_o is the receiver system optical efficiency,
τ_{ND} is the transmittance of the neutral density filters,
S_λ is the detector optical sensitivity (A W^{-1}), and
R_L is the value of the load resistor (in the case of the photomultiplier detectors), or transimpedance (V A^{-1}) (in the case of the avalanche photodiode detector-amplifier).

This equation is useful in itself as it can be used to predict the likely magnitude of the signals measured by the lidar. Because of the very large number of possible system and target configurations, this equation was incorporated into software used to simulate lidar systems.

The laser output energies at some wavelengths were too low to be measured directly because they were heavily attenuated using optical filters in order to enhance the eye safety of the lidar system. However, they could be estimated from the signal measured from a calibrated target at a known range. As the output energy, Q_o, is the integral over time of the laser output power

P(t), the integral of the voltage at the detector output, Σ_V, allows us to calculate this output energy (after all optical attenuation) as

$$Q_o = \Sigma_V \, \pi r^2 \, / \, (\rho \, A_r \, \eta_o \, \tau_{ND} \, S_\lambda \, R_L).$$

Alternatively, if the laser output energy is known, the transmittance of the neutral density filters can be calculated by rearrangement

$$\tau_{ND} = \Sigma_V \, \pi r^2 \, / \, (Q_o \, \rho \, A_r \, \eta_o \, S_\lambda \, R_L).$$

This was the case for measurements at 355 nm where the laser output energy was known but the transmittances of the neutral density filters used in the receiver were too small to be measured by conventional means.

4   Special experimental requirements for the vegetation studies

The very different mode of operation required during the studies of lidar signals from trees, both in the preliminary studies at CAR and in the field at Tanjil Bren, meant that several aspects of the experimental design had to be considered carefully and modified. Because the laser was to be directed at solid targets at close ranges and at low elevation angles, in a region where personnel could be present, laser safety or, rather, the eye safety of personnel in the study, was of prime concern. In addition to concern about the safety of people, there was a considerable concern over the possible damage to the sensitive detectors by strong signals from trees and the calibration target. In addition, enhanced measurement requirements by the EOC had implications on the design and operation of the experiment. These issues are covered in the following sub-sections.

4.1   Laser safety issues

In this section, frequent reference will be made to the latest publication on laser safety by Standards Australia (Laser safety AS/NZ 2211.1:1997, hereafter AS97). Reference to a particular definition or clause (say 3.3) in the standard will be designated in this section in the following way: (AS97-3.3).

Because the output of the laser used in the CAR MWSL could pose a threat to the eye safety of any personnel who accidentally happened to look down the axis of the laser during a pulse, considerable attention has been paid to the design of both the equipment and of the experimental procedures. In the Australian laser safety standards these are known respectively as "engineering" and "administrative" (AS97-3.3) controls.

The laser safety standards define a "maximum permissible exposure" or MPE (AS97-3.51) as "that level of laser radiation to which, under normal circumstances, persons may be exposed without suffering adverse effects". In most laser configurations, the level of laser radiation (power or energy density) decreases with (the square of) the distance from the laser and will eventually fall below the level of the MPE. This is defined as the "nominal ocular hazard distance (NOHD)" (AS97-3.56) or "the distance at which the beam irradiance or beam exposure equals the appropriate corneal maximum permissible exposure." Associated with the

NOHD is a "nominal ocular hazard area (NOHA)" (AS97-3.55) defined as "the area within which the beam irradiance or radiant exposure exceeds the appropriate corneal maximum permissible exposure". The beam exposure or level of laser radiation in pulsed laser systems is usually defined in terms of the quantity "radiant exposure" (AS97-3.64) or "at a point on a surface, the radiant energy incident on an element of surface divided by the area of that element" (usually expressed in $J\ m^{-2}$). The relevant MPEs extracted from Table 7 of AS97 are listed below.

Table 1. Maximum Permissible Exposures (MPE) for intrabeam viewing for various wavelength ranges and pulse durations (t).

Wavelength Range (nm)	Pulse Duration (s)	MPE ($J\ m^{-2}$)
315 – 400	10^{-9} - 10	$5600\ t^{0.25}$
400 – 550	10^{-9} - 1.8×10^{-5}	0.005
1050 – 1400	10^{-9} - 5×10^{-5}	0.05

The equations relevant to the calculation of various lidar design parameters are presented here. From AS97 Equation A5(1), the irradiance at range r (in $W\ m^{-2}$) is

$$E = 4\ P_o\ e^{-\mu r} / [\pi\ (a + r\phi)^2],$$

and from AS97-3.64 the radiant exposure (in $J\ m^{-2}$) is

$$H = dQ\ /\ dA = 4\ Q_o\ e^{-\mu r} / [\pi(a + r\phi)^2],$$

where

P_o is the output power (W),
a is the laser beam diameter at the 1/e points (m),
ϕ is the laser divergence (radians),
Q_o is the laser output energy (J), and
μ is the atmospheric attenuation coefficient (m^{-1}).

As the ranges being considered here are relatively small, the atmospheric attenuation can be neglected. If the laser output beam is not Gaussian in profile, then these quantities should be increased by a factor of 2.5 (AS97-A5). The equation for radiant exposure then becomes

$$H = dQ\ /\ dA = 10\ Q_o\ / [\pi(a + r\phi)^2].$$

By equating the radiant exposure to the maximum permissible exposure, the nominal ocular hazard distance can be expressed

$$NOHD = 1/\phi\ [(10Q_o\ /\ (\pi\ MPE))^{0.5} - a],$$

or, for a Gaussian beam profile (AS97 Supplement 1 Equation 17),

$$NOHD = 1/\phi\ [(4Qo\ /\ (\pi\ MPE))^{0.5} - a].$$

If the beam diameter is larger than the first term in the square brackets then the NOHD is negative and the laser is safe for that exposure at all distances (AS97 Supplement 1-9.2). This can be achieved in some cases by increasing the laser diameter with a beam expander or collimator. A beam expander was designed and built and used for most of the Tanjil Bren field trial and the experiments at Aspendale during December 1999. It increased the beam diameter to 50 mm and decreased the beam divergence to 0.06 mr.

In the following, the MPE and NOHD are calculated for various configurations of the lidar and for all transmitted wavelengths. The energies listed in the first row for each wavelength are the maximum achievable outputs at that wavelength. Note that some of the 1064-nm output is used to produce the 532-nm radiation, and some of both the 1064-nm and 532-nm outputs are used to produce the 355-nm output. In practice all wavelengths are produced simultaneously and, therefore, the output energies at 1064 nm and 532 nm are only about one third to one half of the listed values. The calculations below, therefore, err on the side of caution.

Table 2. Maximum Permissible Exposures (MPE) and Nominal Ocular Hazard Distances (NOHD) for various lidar configurations. Symbols are defined in the text.

Laser Wavelength (nm)	t (ns)	MPE $(J.m^{-2})$	Q (J)	ϕ r	a (m)	NOHD (gauss.) (m)	NOHD (non-gauss.) (m)
1064	8	0.05	0.320	5×10^{-4}	0.006	5697	9015
			6×10^{-7}			0	0.36
			2.5×10^{-7}	6×10^{-5}	0.05	0	0
532	7	0.005	0.155	5×10^{-4}	0.006	12553	19855
			9×10^{-6}			90	139
			4×10^{-7}	6×10^{-5}	0.05	0	0
354.67	6	49	0.08	5×10^{-4}	0.006	79	132
			0.024	6×10^{-5}	0.05	0	0

It can be seen that the NOHD listed in the first row for each wavelength is considerable for 1064 nm and 532 nm. For previous operations in which the lidar has been used for scanning through the atmosphere, a wavelength separator was fitted to reduce the outputs by factors of at least 2×10^{-6} and 6×10^{-5} respectively. The modified (maximum achievable) outputs are shown in the second rows for these wavelengths. The NOHD for all wavelengths is thus reduced to less than about 140 m, which, when combined with the higher elevation angles used in atmospheric studies, and the exclusion of personnel from the NOHA, is a practical

value. The wavelength separator was also fitted during the vegetation experiments at Aspendale and at Tanjil Bren. The last row for all wavelengths shows the result of using the beam expander described below and energies measured during the trial. This shows that the laser output for a single pulse is less than the MPE for all wavelengths, whether or not a Gaussian beam profile is assumed. Indeed, calculations (too detailed to show here) indicate that the MPE criteria are satisfied at all wavelengths even when the laser is fired repetitively.

In addition to the engineering controls mentioned above, the following administrative controls were put in place during the Tanjil Bren field trial:
- the NOHA was conservatively defined as the whole ground area over which the laser was to be scanned at low elevation angles,
- laser safety signs were placed to warn of entry into the NOHA,
- the boundaries of the NOHA were defined by ropes in the region where personnel were operating,
- personnel involved in the study were briefed on the laser operations and their responsibilities,
- the number of personnel admitted to the NOHA was limited to the absolute minimum necessary to accomplish a given task,
- all personnel required to operate in the NOHA were required to wear appropriate laser safety goggles,
- the laser firing direction was monitored using a video camera whenever the laser was operating,
- firing of the laser was at all times under the control of the CAR laser safety officer.

4.2   Detector saturation and non-linearity

The CAR MWSL has the capability to measure signals backscattered from air molecules at an altitude of 50 km. Even in its least sensitive configuration, that used for the measurement of aerosols in the boundary layer at altitudes below 100 m, the lidar is still several orders of magnitude too sensitive to measure signals from solid targets at ranges of 50 m, and damage to the detectors would occur if additional attenuation were not used.

Given the wide range of possible experimental configurations, the peak return signal from solid targets was modelled using modifications to software (PMODEL) used to simulate the performance of various lidar systems, and used in the design of the CAR MWSL. The results confirmed the need for attenuation of the return signal by four to six orders of magnitude. Besides the possibility of damage by very strong signals, somewhat weaker signals can drive the detector into saturation or cause subtle non-linearity problems.

4.3   Implications of enhanced measurement requirements

During the VSIS meeting at the EOC on 16 March 1999, the original request to use the CAR MWSL in a field trial for studying trees was made. However several enhancements were required over the normal operations of the lidar. The most significant of these was the requirement to make measurements at a higher spatial resolution than available with the present system. It was also desired that measurements be made at all three wavelengths and polarisations if possible (although this latter option was not feasible given the limited nature of the study and the limited number of recording channels).

4.3.1 Higher spatial resolution

The requirement for a higher digitiser sampling rate in order to produce a higher spatial resolution had many consequences:

- a faster laser pulse detector was required,
- the laser pulse detector circuit needed rebuilding,
- a separate data acquisition system, control software, display and processing software had to be developed.

4.3.2 Multiwavelength capability

Although the lidar has been used to make atmospheric measurements at three wavelengths, accurate, absolute calibration of the energy monitors and neutral density filters is not usually needed because of the way in which the data are analysed. In the vegetation trials, however, because a relative calibration was not feasible, both the energy monitors and the neutral density filters needed to be calibrated as accurately as possible. New techniques were developed to meet these requirements.

5 Development of new equipment and methods

5.1 Design of the laser beam expander

Detailed calculations were made of the design parameters for a beam expander necessary to achieve an enhancement of the eye safety of the laser used in the vegetation lidar experiments. To minimise cost, standard lenses from the laboratory were used for the task. The radii of curvature and the thicknesses of the lenses were measured in the laboratory, the glass, and hence the refractive index, identified by density measurements, and the performance of the collimator determined using optical ray tracing software.

5.2 Calibration of the neutral density filters

The modelling described in 4.2 confirmed that higher optical density (OD) filters were needed in the vegetation lidar measurements than have been needed in the past atmospheric measurements. The MWSL does incorporate high OD neutral density filters. However, the filters are not truly neutral density and the OD at 355 nm for the strongest filter is nearly two orders of magnitude greater at 355 nm than at 532 nm. This filter is never needed for atmospheric studies at 355 nm and was previously uncalibrated. Several attempts were made to calibrate these filters at 355 nm. However, because the transmittance of the filters at 355 nm is so small, the actual values could not be measured directly. (It is not feasible, nor accurate, to attempt to ratio signals differing by between three and six orders of magnitude.) In the end, best results were obtained by measuring signals from a calibration target at a known range, although these results were limited by the accuracy of calibration of the laser energy monitor.

The new filters for the 1064-nm APD detector could not be calibrated using the available spectrophotometer as the wavelength was outside the available range. After several unsuccessful attempts at calibrations using atmospheric targets, the filters were calibrated directly by measuring the decrease in the laser energy measured by a calorimeter when the filter was inserted into the beam.

5.3 Development of the hybrid data acquisition system

As it was considered that the digitisation rate of the data acquisition system in the MWSL was too low for the vegetation trials, considerable effort was made to develop a suitable system. Because no suitable alternative digitiser could be found as a direct replacement for the existing RTD710A, a hybrid acquisition system was developed. This incorporated a CAR TDS380 2 Gs/s, dual-channel, 8-bit, sampling oscilloscope controlled by a dedicated computer via a General Purpose Interface Bus (GPIB) provided by the EOC and CSIRO Energy and Mining (CEM). As this computer could not access any of the "housekeeping" data available to the MWSL system, both systems were run in parallel. The lidar signals were recorded on the TDS380 system and the shot times, elevation and azimuth angles, laser energies and recorded wavelengths, detector gains and other parameters recorded by the MWSL system. The hybrid system is depicted in Appendix 1. Unfortunately, the signals could not be monitored simultaneously by the CAR system as is usually done because of "ringing" in these fast signals over the long lines used to join the two systems.

During tests of the hybrid system, it was found that the TDS830 system could not record at the laser firing rate, and randomly duplicated files. After much experimentation a divider circuit was designed and interposed between the two systems so that only every fourth profile was recorded by the TDS380.

6 Software developments

Numerous computer programs needed development during the study. Unfortunately the source codes are too long even to be included as appendices, but can be made available by the author on request. They are summarised below.

PMODEL

This lidar simulation program was developed further, first to estimate the maximum signal strengths from solid targets, then to simulate the signals from solid targets using a laser pulse with a Gaussian temporal profile. This was to test the deconvolution software.

PROFIL32

This is the multi-function data analysis and test-bed program used for processing atmospheric lidar profiles. It was further developed to produce summary files of all the relevant recording information associated with the files recorded with the TDS380 system so these data could be analysed. Another development was a high pass filter routine that was used to test algorithms that correct for the limited bandwidth of the recording system.

LPACQ

This program was initially written by CEM, then developed iteratively, in collaboration with CAR, for controlling the recording of data on the TDS380 and transferring data to the control computer via the GPIB.

R_TDS380

LPACQ is basically only a command line program. The program R_TDS380 is a shell program that calls LPACQ and was written to provide the following enhancements:
• the input of the recording parameters is via an explanatory menu,

- the input parameters are checked to ensure that data are not accidentally overwritten,
- recorded data are displayed (and optionally redisplayed) on the monitor allowing some quality control,
- all the profiles in a directory may be viewed automatically, one at a time, after the event.

INTEGR8

This program uses various means to estimate the background level in noisy signals and then integrates the signal after removing the background level. It was used in the analysis of the calibration target data.

DECONV

This program tests the performance of various deconvolution algorithms for correcting recorded signals for the system response function.

CONVDCNV

The performance of numerical filter algorithms in convolving and deconvolving modelled signals is tested with this program.

7 The Tanjil Bren field trial

7.1 Overview

After the system had been calibrated and the new equipment tested, the CAR MWSL was deployed to the field site near Tanjil Bren, arriving late afternoon on December 6th. Unpacking and setting up was completed the next morning. Several hours were lost next day in the repair of a damaged cooling fan in the laser power supply and while attempts were made to rectify a fault that had developed in the circuitry and cabling that monitored which optical filters were being used. This problem was only partly resolved and led to inaccurate recording of some laser energy information. The EHT unit that supplies the 355-nm detector also developed a minor fault during transport and could not be repaired in the field. This led to calibration uncertainties that required correction after the field trip.

With the delays mentioned above, recording of data was not begun until 1800 LT on December 7th, and only a small amount of useful data was acquired before it was too dark to operate. One striking feature of the recording at night time, however, was the very noticeable fluorescence from many of the vegetation targets. The 355-nm beam is quite invisible but the laser spot could be seen quite clearly on some of the trees. The study was continued into the second day with useful data being acquired on a variety of trees and the calibration target. The data quality was generally good despite problems associated with the high ambient temperatures affecting the energy monitors and detector sensitivities, and the bright sky background signal causing overload and possible damage to one of the detectors. Measurements ceased and packing up began in the afternoon of December 8th.

After the field trip, the data were checked for consistency and quite some time was spent attempting to develop a consistent calibration of the signals. Despite uncertainties caused by the problems mentioned above, this was achieved in most cases. The data, along with summary and explanatory text files, are archived on the EOC ftp site as described below.

7.2   The location

The Tanjil Bren site was selected for the field trial because many of the stands of trees in the area had been characterised previously and the area was used for forestry research. The remoteness of the site provided more security for the equipment and also reduced the chance of interruptions to operations by the unannounced arrival into the study area of other people or vehicles. However, the long, steep and rough logging track probably contributed to some of the problems encountered with the equipment. The site was located near the top of Regnans Road off the main Noojee – Tanjil Bren road. Figure 3 is a map of the study area with various labels indicating stands of trees that have been the subjects of previous studies. The lidar was located in the cleared area near the top of the figure, between the labels "3" and "20a". Most of the lidar data were acquired from trees near the area labelled "8" with some in an area near the label "3". Some signals were also measured from dead trees near the label "20 a". A closer view of the lidar site is shown in Figure 4. The lidar is located at the centre of the circle with the line to the south west indicating the range and bearing to the calibration target. This "Spectralon" panel was located at a distance of 89 m and on a true bearing of 200 degrees. Figure 5 is a photograph of the lidar caravan on site with the target trees in the background.
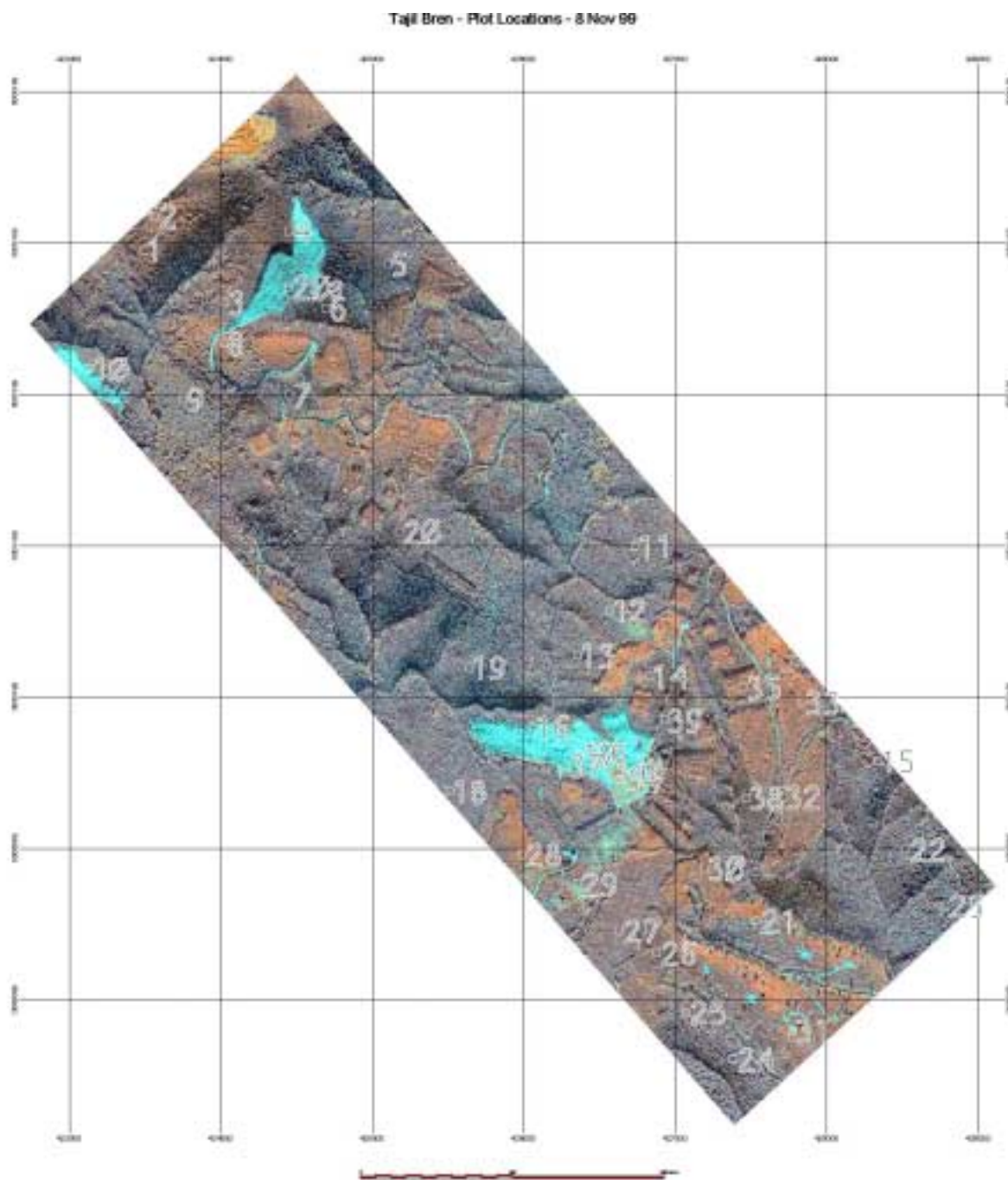
Figure 3. A map of the vegetation lidar study area near Tanjil Bren. The lidar was located in the clearing near the top of the figure. Stands of trees characterised in forestry studies are labelled. Regnans Road leaves the main Tanjil Bren – Noojee road just to the right of the label "20". Australian Map Grid (AMG) coordinates are shown.

Tanjil Bren
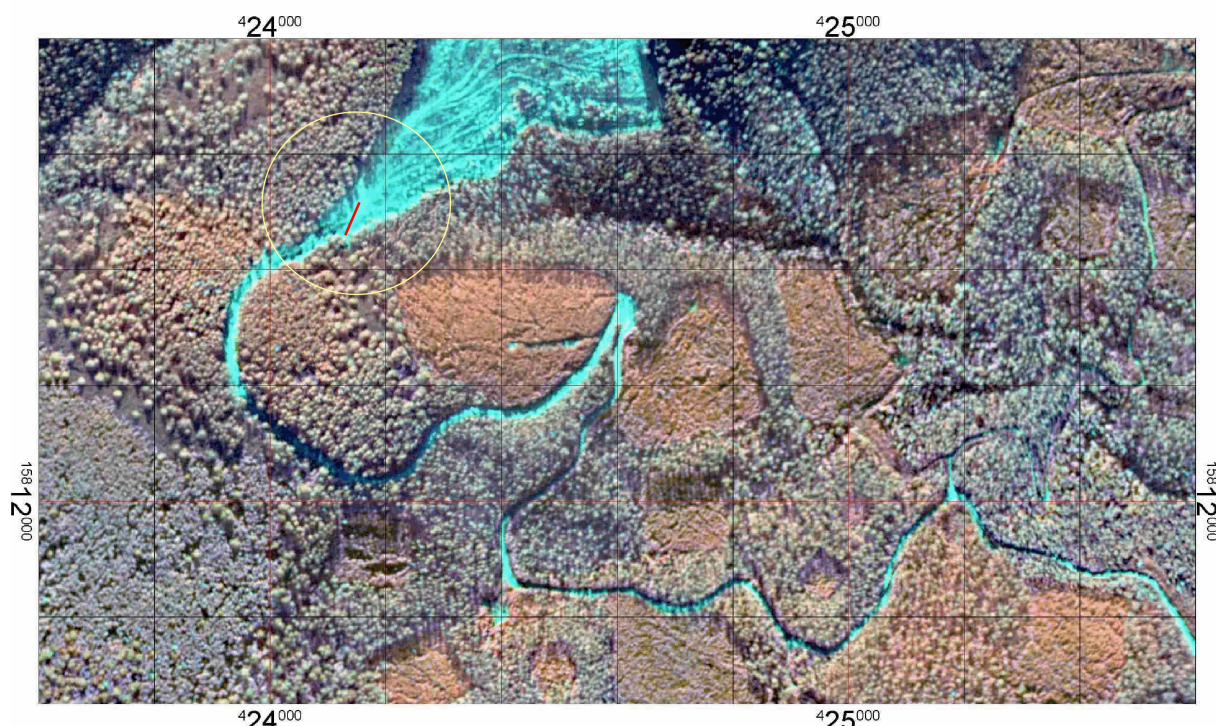
Figure 4. A finer scale map of the study area. The lidar was located at the centre of the circle. The line indicates the range and bearing of the Spectralon calibration target. AMG coordinates are shown.

7.3　Experimental details

Before any data were recorded, the laser output energy at 355 nm was maximised by tuning the harmonic generator. The energy at 355 nm was checked using the laser calorimeter, and the reading on the optical pulse energy monitor recorded for all wavelengths. Note that the measurement of output energies at 532 nm and 1064 nm with the calorimeter requires an experimental setup that is too complicated to set up in a reasonable time in the field. Also, after passing through the wavelength separator, the energies at these wavelengths are about four or more orders of magnitude too small to be measured using the calorimeter. It was assumed that the calibrated relationships between the output energies at these wavelengths and the readings on the optical pulse energy monitor measured at Aspendale prior to the field trip were maintained throughout the experiment. As the daytime temperatures exceeded the upper limit of its temperature control circuitry, considerable drifts occurred in the tuning of the harmonic generator, with a consequent change in the output energies at the various wavelengths. Therefore, the harmonic generator was tuned frequently and the outputs of the pulse energy monitor noted.

The data recording systems were set up with the CAR system recording all the setting parameters and the TDS380 system recording every fourth signal along with the corresponding shot time as determined by the EOC computer. Although the EOC PC and the CAR control PC were manually synchronised, the time stamps on the files recorded by both systems drifted considerably during the recording periods. For example, the clocks were

16

Figure 5. A view of the Tanjil Bren field site looking to the south west. The CAR lidar caravan is seen attached to the truck that carries the 240 V generator. Lidar signals were recorded mainly from the trees in the background, although some signals were recorded from the dead trees to the left and the tall trees on the right. Two levels of vegetation canopy can be seen. The taller trees are *Eucalyptus regnans* (Mountain Ash).

synchronised manually at 0936 LT on December 8th. The times were checked again at 1354 according to the reference and found to differ by less than 0.2 seconds, a time difference that is comparable to the reaction times of the personnel involved. However, on one of the files the difference in recorded times is 9.6 seconds at 1143 and increases to 17.3 seconds at 1243. This difference would seem to be inconsistent with the previous efforts at synchronisation and is unexplained at this stage. It will add a little more complexity to the task of correlating the record header information recorded with the CAR system and the files recorded with the EOC system.

Before any measurements were made of signals from the trees, several sets of data were recorded using the various detector channels and the lidar signal from a calibration target. The target was a "Spectralon" panel set up at a distance of 89 m from the lidar at the base of some trees that were to be studied. It has a reflectance of close to 0.99 for all the wavelengths used in the study. In addition to providing a useful check on the calibration of various optical parameters in the system, it gives the temporal response function of the lidar system on any channel. This is the function that is needed if efforts are to be made to deconvolve the recorded data for the effects of laser pulse length, the time response of the detector and the

bandwidth of the recording system. This was recorded on several occasions on both days to track the consistency of the calibration of the lidar.

The method of sampling data from the trees is now described. First the lidar was scanned manually with the laser firing continuously and the return signals displayed on the TDS380 to allow the scan pattern to be defined and the settings on the TDS380 to be optimised. Because the signals varied over a wide range of amplitudes, and the 8-bit digitiser only has 256 recording levels, it was not possible to record all signals in a scan optimally, but an effort was made to keep the strongest signals on scale. The lidar was then set into the automatic recording mode. In this mode the lidar is scanned in elevation at a steady rate, which is calculated to record data at a series of elevation angles that are separated by the increment selected by the operator, while allowing the laser to fire at its optimum rate of ten shots per second. The angle increment at Tanjil Bren was either 0.3 or 0.5 degrees, depending on the total elevation angle to be covered. Note that the TDS380 system could only record every fourth record so the actual recording increment was 1.2 or 2.0 degrees. This is very coarse and under-samples the target considerably, but it was the best result achievable with the hybrid system. The scanning methodology is depicted in Figure 6. In order to estimate the variability in a scan caused by movement of the target in the wind and other variations, the elevation scan at any particular azimuth angle was repeated up to five times. Elevation scans were then made at other azimuth angles in order to measure variations in the vegetation structure in the horizontal direction.

The nearest trees in any azimuth angle being studied varied in range from 60 m to 120 m. As the total recording range of the TDS380 at its maximum recording rate of 2Gs/s is only 75 m, it was necessary to set a delay between the triggering of the TDS380 and the first data point. Sometimes the spread in range of the signals recorded in any elevation scan was greater than 75 m and a coarser sampling interval and different delays were used. Unfortunately, unlike the MWSL recording system, the LPACQ software did not record the delay time or include the delay in the time variable in the output files. This means that the range to the target cannot be determined from the data alone. Fortunately, many of the delays were manually noted in the operator's log and aerial photographs of the site were used to estimate the range to the nearest trees for all of the scans. These data are included in the summary files and will reduce the uncertainty in the range information.
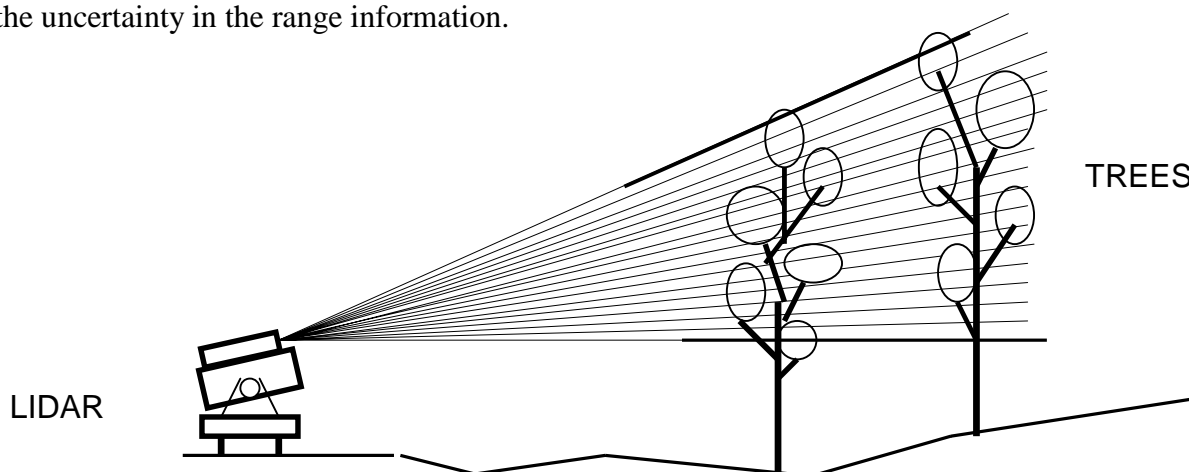
Figure 6. The methodology used in sampling trees with the lidar. The lidar is scanned upwards through a range of elevation angles while the laser is firing and signals are recorded at these angles. The darker regions shown on the minimum and maximum angles indicate the ranges over which signals are recorded.

7.4 Illustrative examples of the lidar data

7.4.1 Signals from the calibration target

As described above, frequent measurements were made of signals reflected from the calibration target. These provide data on the temporal response of the lidar system in any detector channel and also enable checks to be made on the calibration of the lidar.

An example of signals recorded from the calibration target is shown in Figure 7. The target was at a range of 88.8 m and a delay of 544.5 ns was set on the TDS380. The positive-going signal is from the avalanche photodiode (APD) detector used for recording 1064-nm data, while the smaller, negative-going signal is the 355-nm return from one of the photomultiplier tubes (PMTs). The different timings for the peak signals on each channel results from the approximately 50 ns transit time of photoelectrons through the multiplier stage of the PMT. The apparent secondary hump in the APD signal at 160 ns is unexplained and may be a reflection in the signal cable, although these were terminated with low tolerance 50-ohm loads. Alternatively, it may be a detector effect. Eight consecutive 1064-nm signals from the APD are plotted in Figure 8 illustrating the very small shot-to-shot variation in the lidar output pulse temporal profile. The implication from this result is that the corresponding laser output pulse does not need to be recorded for each signal from the vegetation canopy.
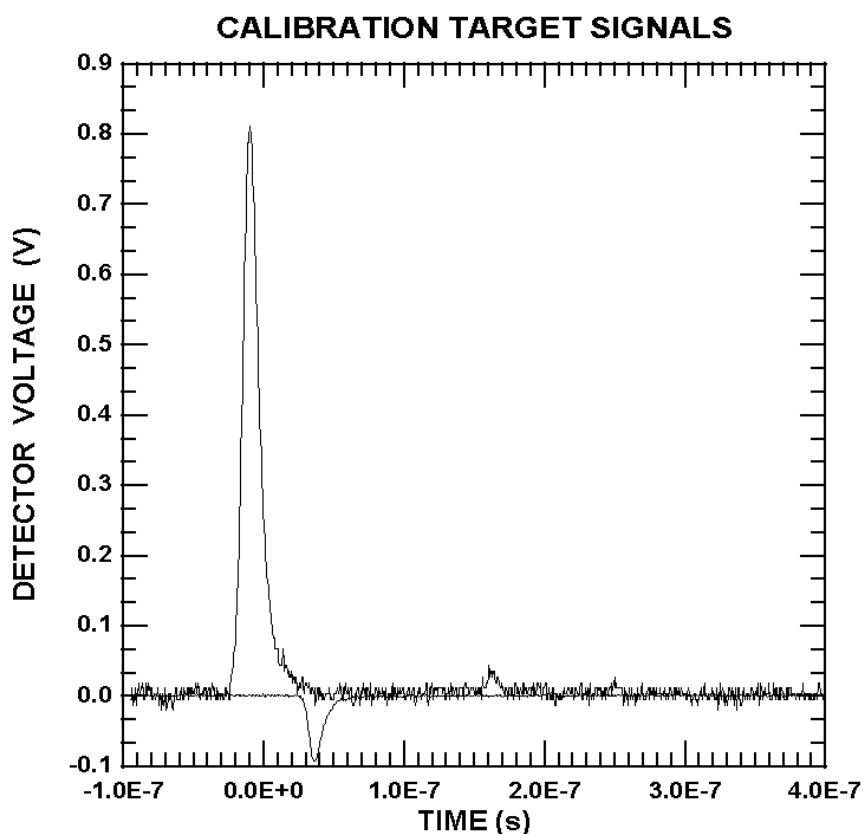
Figure 7. Signals recorded from the calibration target at 88.8 m range with a digitiser delay of 544.5 ns. The positive-going signal is the 1064-nm return while the 355-nm signal is negative-going. The time axis covers a range of 500 ns or 75 m.
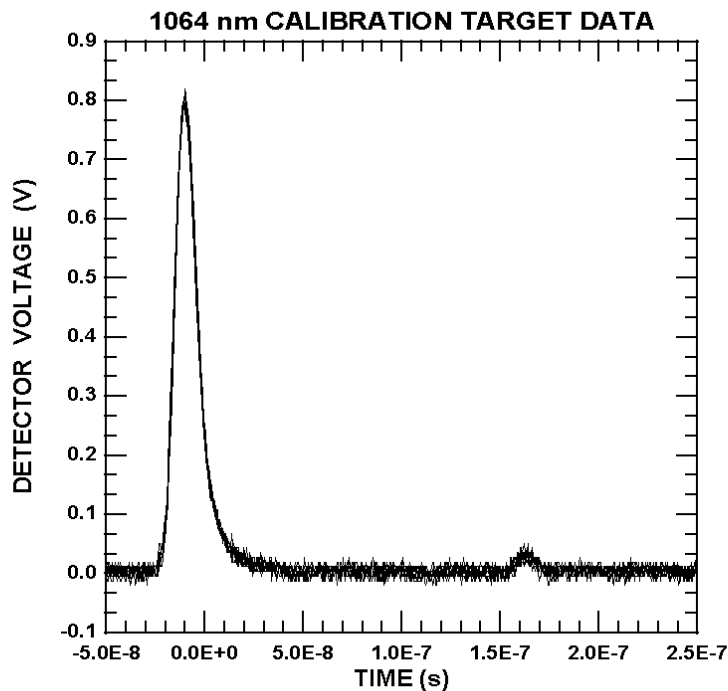
Figure 8. Signals recorded from the calibration target at 88.8 m range with a digitiser delay of 544.5 ns. All eight 1064-nm APD signals recorded by the TDS380 in a 32 shot burst of laser shots are overplotted here and demonstrate the shot-to-shot consistency in the laser temporal profile.
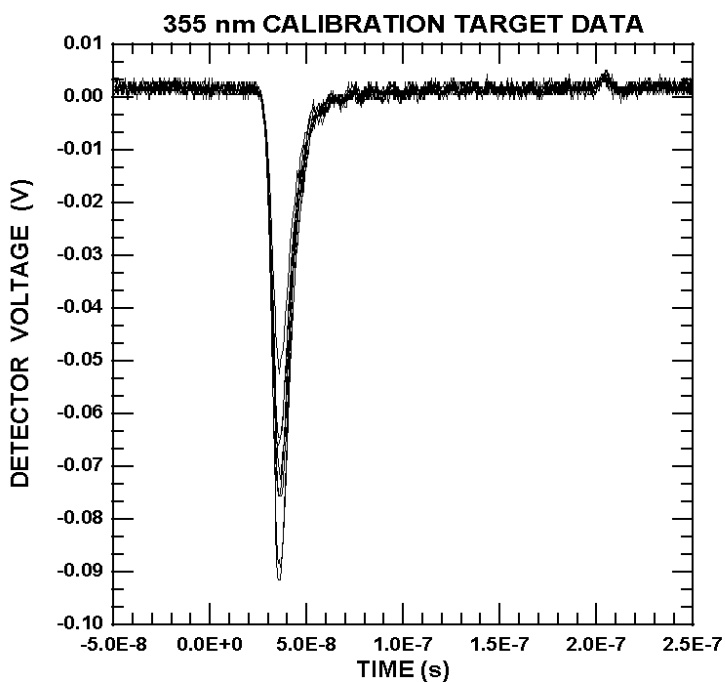
Figure 9. Signals recorded from the calibration target at 88.8 m range with a digitiser delay of 544.5 ns. All eight 355-nm PMT signals recorded by the TDS380 in a 32 shot burst of laser shots are overplotted here and demonstrate the shot-to-shot consistency in the laser temporal profile, even though the magnitude varies.
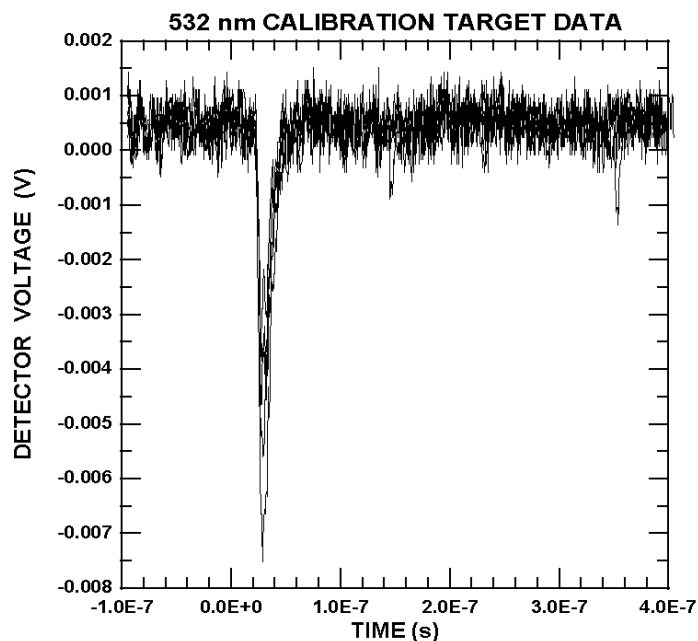
Figure 10. Signals recorded from the calibration target at 88.8 m range with a digitiser delay of 544.5 ns. All eight 532-nm PMT signals recorded by the TDS 380 in a 32 shot burst of laser shots are overplotted here and demonstrate the shot-to-shot consistency in the laser temporal profile.

Calibration data for 355 nm and 532 nm are plotted in Figures 9 and 10 respectively. It can be seen that the temporal profile also remains consistent for these wavelengths, although the actual laser output energy varies from shot to shot. This is a result of the variation of the output energy at the two higher harmonics while the laser "warms up" during a short burst of shots. The third harmonic energy depends on the output energy of both the lower harmonics. Note that these signals have not been normalised for variations in the output energy as is usually done. The signal to noise ratio (SNR) for the 532-nm signal is poorer than for the other wavelengths because the neutral density filter, which is common to both channels, was optimised for the 355-nm signal. Remember that the 532-nm output energy has already been reduced by about five orders of magnitude by the wavelength separator, and the neutral density filter in the detector unit reduces it by almost another three orders.

7.4.2   Signals from the vegetation canopy

As described above, the vegetation canopy was sampled by scanning the lidar in elevation and measuring the reflected laser signals from the targets along the laser path. Because there were only two input channels on the digitiser, simultaneous measurements could only be made at two of the three available wavelengths. Because the neutral density filters were common to the 532-nm and 355-nm channels, and the filter was optimised for measurements at the latter wavelength, either 1064 nm and 532 nm, or the 1064-nm and 355-nm combination of wavelengths was used, as these gave the best results. (Unfortunately problems with the 1064-nm detector meant that only the 355-nm and 532-nm combination could be used on the second day.) The RTD710A digitiser in the MWSL achieves a high data recording rate by storing bursts of shots in its internal buffer. For the record length usually employed, a maximum of 128 shots can be stored when operating in single-channel mode or 64 shots in

dual-channel mode used throughout the study. With the sub-sampling described above, this translates into a maximum of 16 recorded profiles at each wavelength for each scan.

The signals recorded at 532 nm during an elevation scan through the vegetation canopy are plotted in Figure 11. The corresponding data for 1064 nm are plotted in Figure 12. The range of elevation angles covered was from 4 degrees to 20.5 degrees with a step of 1.2 degrees. All signals are plotted on the same range axis, so signals from a target at a constant horizontal distance, but measured at higher elevations, will appear displaced to the right on the plot. The spiky nature of the signals and the large dynamic range are immediately apparent. This results from the small (50 mm) spot size of the laser footprint on the target. The poorer SNR in the 532-nm data when compared with the target data is a result of the bright sky background at high elevation angles and the very wide receiver field of view that was required in order to detect signals at such a close range. (Also, the filter in the 1064-nm channel was still optimised for recording signals from the target. A lower optical density (OD) would have produced a better SNR.) The weaker signals recorded at some angles have been masked in the plots by the noise at other angles. Some signals recorded at elevations where there was no vegetation target have been excluded from Figure 11 because the bright sky background makes them too noisy. The data in Figure 13 are the signals recorded at 355 nm. Although these signals were not recorded simultaneously with the data in Figures 11 and 12, they were recorded with the lidar pointing in the same directions. The superior SNR can be seen in these signals.

As a final example of the signals measured from the vegetation canopy, four pairs of signals are plotted in figure 14. These show the 1064-nm data plotted in the positive direction and the 355-nm data plotted in the negative direction. The time delay between the corresponding signals at the different wavelengths has been explained above. Of particular interest is the
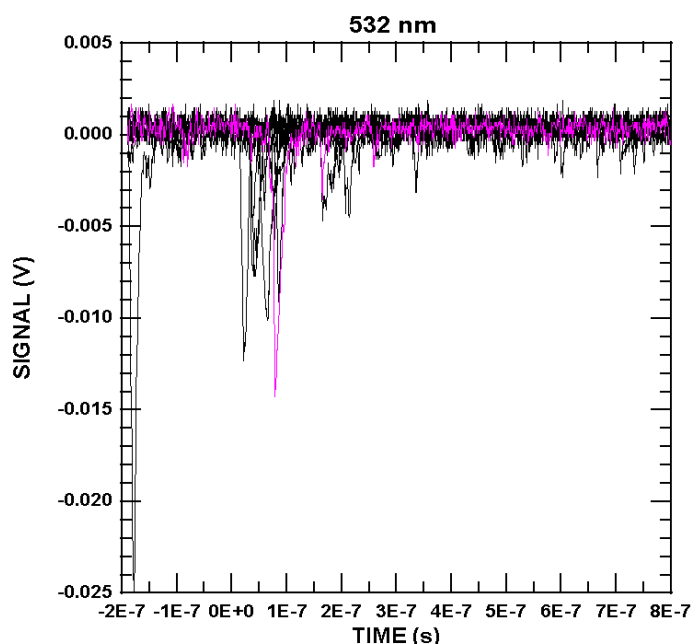
Figure 11. Signals recorded in an elevation scan through the vegetation canopy at an azimuth angle of 197.4 degrees. The range interval is 150 m and the nearest target is approximately 96 m from the lidar.

dramatic change in the relative signal strengths measured for different targets and different wavelengths. Compare, for example, the difference in the pairs marked A and B. In A the signals measured at both wavelengths are single pulses of comparable magnitudes. In B there is a double echo of comparable magnitude at 1064 nm but the second pulse is much stronger in the 355-nm return. The relative differences in pair C is even greater. Also note that the signals at both wavelengths are comparable in A, the 1064-nm signal is greater in D, but the 355-nm signal is greater in C.
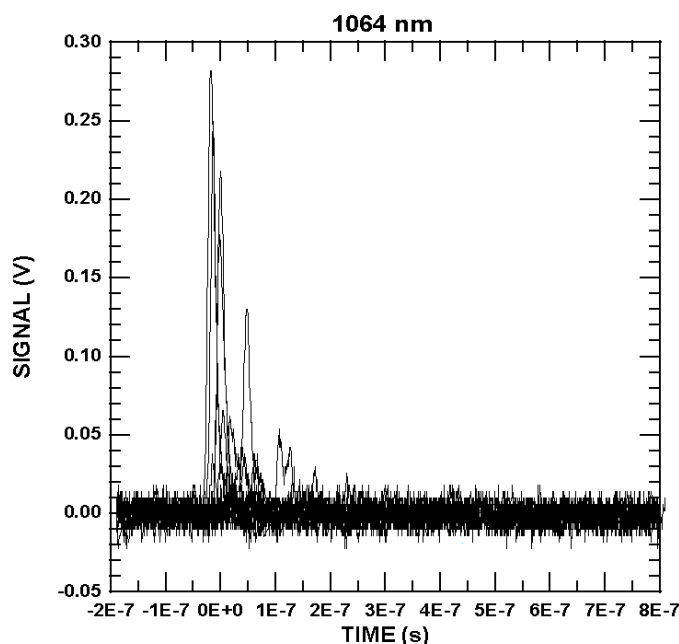
Figure 12. Signal recorded at 1064 nm simultaneously with the data in Figure 11

7.5 Interpretation of the lidar measurements

7.5.1 Calibration data

The signals from the target were used for the following purposes:
- to provide a calibration of the range delays,
- to measure the system temporal response for all three detectors,
- to estimate the laser output energies at 1064 nm and 532 nm,
- to estimate the optical density of the neutral density filters used at 355 nm.

There are several delays in the recording of the lidar signals. The photoelectron transit time in the PMTs has already been mentioned. There are also different electrical cable lengths between the trigger circuits and the signal circuits and there is an electronic pulse counter or divider circuit on the trigger line for the TDS380 and EOC computer. There are, then, delays in both the trigger and signal lines. The difference between these determines the net delay used in calculating the range to the target and this was determined using the target signals.

The distance to the target was measured using a tape measure as 88.8 m. Given the undulating terrain, this measurement is probably only accurate to about 1 %. With the TDS380 trigger
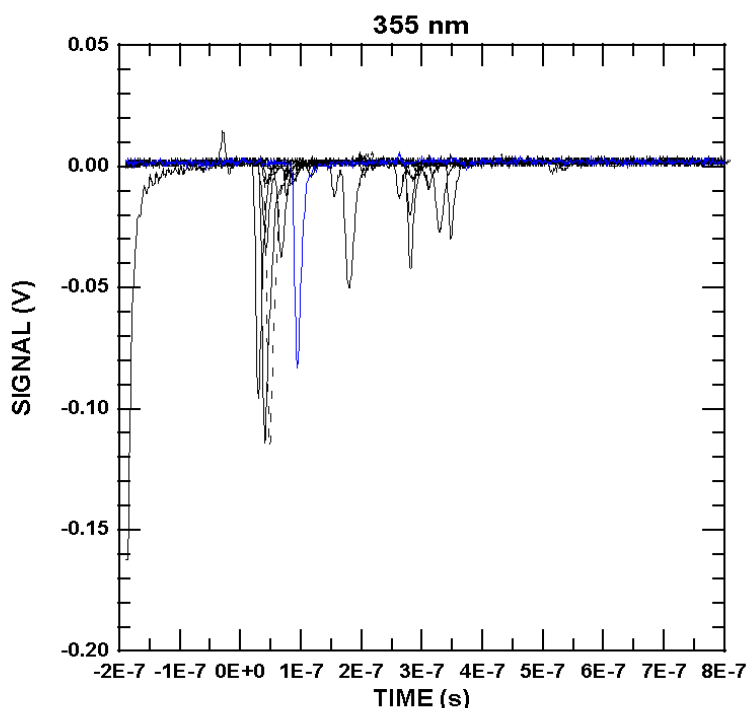
Figure 13. Signals recorded at 355nm at the same elevations as the data in Figures 11 and 12.

delay set at 544.5 ns, the recorded time to the target was –10 ns for the 1064-nm APD detector, +30 ns for the 532-nm PMT and +35 ns for the 355-nm detector. (The 532-nm PMT was operated at a higher voltage and gain than that for 355-nm and this resulted in a shorter transit time.) The net delay times are then –57.5 ns, -47.5 ns and –47 ns for the 1064-nm, 532-nm and 355-nm signals respectively. (The negative values mean that the electronic delays in the trigger circuit dominate the delays in the signal lines.)

The output energies at 1064 nm and 532 nm, after attenuation by the wavelength separator, were too low to be measured directly with the calorimeter. During the experiment, the outputs of the pulse energy monitor were used with estimates of the upper limits of the transmittances of the wavelength separator to estimate the actual laser energy transmitted to the target. (The pulse energy monitor had been calibrated previously using the calorimeter and the unattenuated laser energies.) Analysis of the signals from the calibration target provided a means of checking these energies. The program INTEGR8 was used to calculate the background level in the signal by analysing the histogram of the digitisation levels in the data. This level was then removed from the signal and the area under the pulse integrated. The average values in each set of bursts were calculated and used with the system data in Table 3 and the equations derived in Section 3 to calculate the output energies. The results of the energy calculations are presented in Table 4 for 532 nm and in Table 5 for 1064 nm. The 532-nm measurements cover both observation days and indicate the variation over that period.

Table 3. Lidar system data. The symbols are defined in the text. '?' values are to be determined

Parameter			
Wavelength (nm)	355	532	1064
S_λ (AW^{-1})	214 @ 1250 V	4.27×10^4 @ 1750 V	35
η_o	0.325	0.413	0.2375
ρ	0.986	0.99	0.988
Q_o (J)	0.024	?	?
R_L (VA^{-1})	50	50	10^5

Table 4. Laser output energy calculations at 532 nm. Symbols are defined in the text.

Data Sequence	Σ_V (V s)	ND filters	τ_{ND}	Q_o (J) x 10^{-7}
/003/t01_1 -- 47	1.04×10^{-10}	'3'	3.45×10^{-3}	4.46
/003/t01_49 -- 63	5.65×10^{-10}	'2, .3'	2.25×10^{-2}	3.71
/007/t04_1 -- 15	2.46×10^{-11}	'3, .5'	1.06×10^{-3}	3.43
/007/t04_17 -- 47	4.83×10^{-11}	'3, .1'	2.44×10^{-3}	2.93
/009/t05_1 -- 15	1.15×10^{-10}	'3'	3.45×10^{-3}	4.93
/010/t06_17 -- 31	2.85×10^{-10}	'2, .5'	1.3×10^{-2}	3.24
			Mean	(3.78 ± 0.31)

Table 5. Laser output energy calculations at 1064 nm. Symbols are defined in the text.

Data Sequence	Σ_V (V s)	ND filters	τ_{ND}	Q_o (J) x 10^{-7}
/001/t01_1 -- 15	1.27×10^{-8}	'1'	1.87×10^{-2}	2.13
/003/t01_1 -- 15	1.31×10^{-8}	'1'	1.87×10^{-2}	2.20
/003/t04_50 -- 64	1.39×10^{-8}	'1'	1.87×10^{-2}	2.33
			Mean	(2.22 ± 0.06)

As explained above, direct measurement of the attenuation of the neutral density filters used at 355 nm was not possible. The strongest filter was calibrated using the target data and the equations derived above. The results are summarised in Table 6. Two sets of measurements were made with additional filters in the optical path. The signals for these experiments are quite inconsistent with the others and may result from an unresolved uncertainty in the filter settings. These data are excluded from the means. Otherwise the variations in the calibration over the experiment seems acceptable.

Table 6. Transmittance calculations at 355 nm for the neutral density (ND) filter '3'. Some data were recorded using additional ND filters as indicated in column 3. OD is Optical Density. Other symbols defined in the text.

Data Sequence	Σ_V (V s)	ND filters	τ_{ND} x 10^{-6}	OD
/001/t01_02 -- 16	1.08×10^{-9}	' .5'	2.29	5.640
/002/t01_02 -- 16	1.06×10^{-9}	'.1'	2.23	5.652
/003/t01_02 -- 48	1.03×10^{-9}		2.23	5.652
/007/t04_02 -- 16	2.81×10^{-10}		9.27	5.033 *
/007/t04_34 – 48	1.65×10^{-9}		7.38	5.132 *
/009/t05_02 – 16	1.19×10^{-9}		2.43	5.614
	Means excluding *		(2.30 ± 0.05)	5.639

7.5.2 *Vegetation signals.*

The dramatic variability in the signals at the different wavelengths presented above is the result of several factors. The most obvious is that the reflectivity of the vegetation targets is strongly dependent on wavelength. Another possible factor is that the targets fluoresce when illuminated with the ultraviolet 355-nm radiation. As the MWSL only has receiver channels that match the three transmitted wavelengths, it is not possible to make conclusive measurements of the amount of fluorescence radiation in any channel. A separate receiver channel operating at another independent wavelength would be needed for that purpose. However, the laser beam was observed hitting the targets, both visually and with the television monitor, during the measurements on the night of December 7th. As the laser radiation is invisible, what was being observed must have been fluorescence. One other factor is related to the slight change in the proportion of laser energy transmitted at each wavelength as the laser "warms up" during a burst of shots. This would produce an apparent shot-to-shot change in the ratio of the signals at different wavelengths plotted in Figure 14, which are raw data and are uncorrected for energy variations. However, the change of the relative ratios in those signals where there is more than one echo demonstrates that the effect is real.
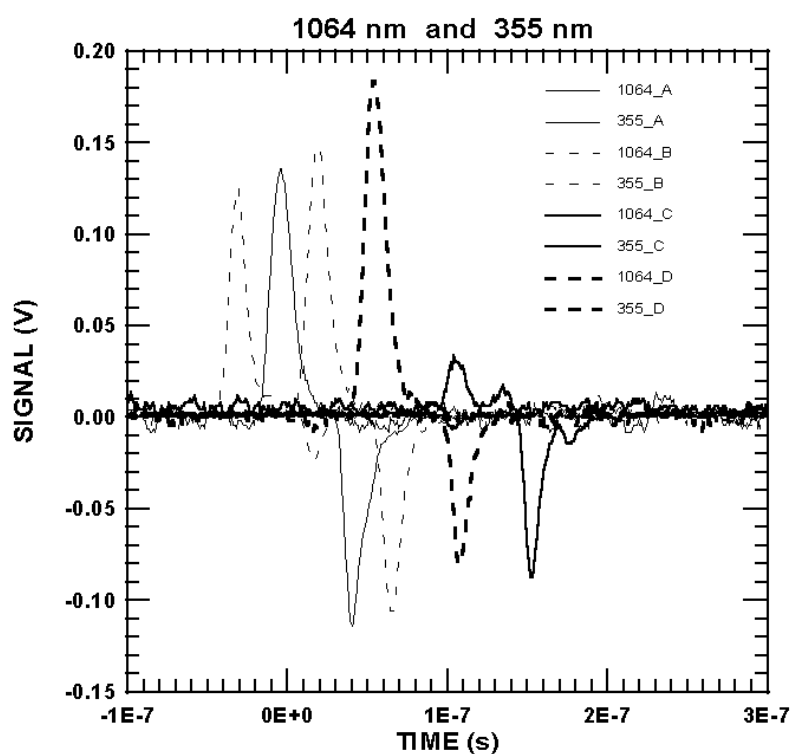
Figure 14. Four pairs of signals recorded simultaneously using different wavelengths. The 1064-nm signals are positive while the 355-nm signals are negative. Signal pairs are plotted using the same line style. Note the changes in the relative signals in the different pairs and also the relative differences in the pulse structures.

8 Description and availability of the data set

The data recorded during the Tanjil Bren experiment, and also data recorded during an experiment at Aspendale on December 2nd, have been archived and placed on the EOC ftp site. The address is ftp.eoc.csiro.au and the directory is ftp/pub/veglid. The username is veglid and the password must be obtained from the EOC.

8.1 The data summary files

The Tanjil Bren data are stored in a series of subdirectories starting with /001/ and ending with /010/. There are also jpeg picture files stored in a directory /pix/. Data recorded at Aspendale are stored in the directory /car/. A set of list files is located in the directory /mwsl/. These files list all the relevant header information recorded by the MWSL data acquisition system and are needed for the interpretation of the data recorded using the EOC system. They contain details of the laser wavelength used and laser energy, the neutral density filters in the channels, the elevation and azimuth of the record, and the laser shot time to the nearest 0.1 seconds.

27

The following files are stored in the root directory and give a detailed description of the contents of all the directories, what is on the files and some caveats.

VLREADME.TXT

A brief description of the experiment is given along with the contents of the directories, the location of the data and what was measured.

LID_SUM.XLS

This is a MS Excel file that lists all the data files recorded with the TDS380 / EOC system using the CAT software. The linking between these files and the header information recorded with the CAR MWSL, and information on what was measured, where the lidar was pointing and so on is given.

VIDEOTAP.TXT

This file summarises the contents of the two videotape records of what the lidar was recording during the Tanjil Bren experiment. The tapes can be used to trace exactly where the lidar was pointing for a particular laser shot.

TDS_DATA.TXT

This file lists all the TDS data and essential information as to where they are located and what information is on the files and the data format.

9   Conclusions and recommendations

The vegetation lidar studies reported here have been successful in acquiring useful data that illustrate a number of important aspects of the measurement of lidar signals from vegetation. These points should be considered carefully during the design of a dedicated vegetation lidar system. Among the most important are those relating to the sampling strategy, laser energies, pulse lengths, digitiser speed and dynamic range and the selection of the operating wavelengths.

The selection of an appropriate sampling scheme has profound implications for many aspects of the design of the lidar system. The narrow beam (50 mm), coarse angular resolution (1.2 degrees) and close range of the targets (90 m) used in the Tanjil Bren trial meant that the structure of the vegetation canopy was grossly under-sampled. (The effect is similar to aliasing.) The small laser 'footprint' on the target also causes very spiky signals. These signals are just the convolution of the system temporal response function with the series of delta functions that represents the ranges of all the targets intercepted by the laser pulse along its path. The resulting signal has a very large dynamic range. It ranges from the weakest grazing encounter of a low reflectance leaf at a high incident angle by a pulse that is already attenuated by previous encounters along its path, to the total obstruction and reflection of an unattenuated pulse by a high reflectance tree trunk. The digitiser needs to be able to measure both signals adequately using the same input range as the size of the signal is not known beforehand. Although logarithmic signal compression can be used in some circumstances, most of these amplifiers do not have the accuracy, stability or bandwidth for this application. The conclusion is that the narrow beam imposes very high demands on the digitisation system. The combination of a bandwidth of about 1 GHz, a sampling rate of 1 to 2 G samples per second with at least two input channels and an amplitude range of greater than 8 bits may

be difficult (or expensive) to achieve. The data transfer rate from the digitiser to the computer is another important parameter as it determines the sampling over the target space. The transfer rate available with the hybrid system used here (about two records per second) led to significant under-sampling of the target. A broader laser footprint would help to alleviate many of these problems. It would reduce the required recording and transfer rate by performing a lateral integration over the target. The broader pulse would also encounter more scatterers for each unit of distance that it encounters. By this in-pulse integration, the spiky nature of the signal would be replaced by a more slowly varying signal with a much reduced dynamic range. The broader footprint, achieved by using a diverging laser beam, would need to be considered along with the field of view of the receiver. Because the transmitter and receiver axes in the MWSL are separated, a very large receiver field of view was needed to allow the measurement of signals from the close target range used. A coaxial system would permit the use of a smaller field of view, but still sufficient to encompass the laser footprint, and the resulting signal-to-noise ratio would be considerably improved. The requirements on the digitisation system can thus be considerably reduced by a careful selection of the design parameters discussed here.

The MWSL used in the study was designed by the author for measurements of signals backscattered from atmospheric targets such as clouds, air molecules and aerosols at ranges of up to 50 km. These atmospheric targets scatter relatively weakly and the lidar needs a laser of high power to produce measurable signals. For the vegetation studies reported here, the output energy of the laser was attenuated by 2×10^{-6} at 1064 nm and the return signal was further attenuated by another factor of 0.02 and the signal was still close to saturating the APD detector. Similarly, the 532-nm output was attenuated by a factor of 6×10^{-5} and the return signal by another two to three orders and the signal was still measurable. At 355 nm the approximately 24 mJ output was unattenuated but the return signal needed attenuation by almost six orders of magnitude. Acceptable signals would therefore have been obtained from the targets at 100 m range with the present 0.35 m receiver and unfiltered detectors with approximate laser energies of 4 nJ at 1064 nm, 9 nJ at 532 nm and 80 nJ at 355 nm. The very important conclusion from these estimates is that a completely eyesafe, multiwavelength vegetation lidar system could be built around the proven and reliable Nd:YAG laser technology. The use of a diode-pumped system would lead to both higher efficiencies and the higher achievable laser firing rates desirable for an airborne system. A laser with a short pulse length is also desirable. Although attempts can be made to deconvolve the signal for the system temporal response (mainly the laser pulse shape) these efforts are usually hampered by noise in the signal, and it is far easier to begin with a short laser pulse length at the outset.

Finally, the selection of laser wavelengths needs consideration. The field trials demonstrated that good signals were measured at all the wavelengths used. These wavelengths include those used by current systems such as SLICER and by the VCL instrument that is due for launch in September 2000. Any vegetation lidar system designed in Australia could benefit from using the same wavelength as the VCL, as this would enable more direct validation of the VCL data as well as the development and testing of algorithms for the analysis of VCL data from Australian trees. The benefit of using multiple wavelengths was demonstrated in this study. The different signals measured simultaneously at the different wavelengths are related directly to the reflectivity of the targets. Analysis of these differences would give information on the nature and type of vegetation being measured. The use of an ultraviolet transmission wavelength with an on-line receiver channel and at least one receiver channel measuring fluorescence signals could also provide valuable information on the type and vitality of the vegetation target.

10   Acknowledgments

11   References

Baltsavias, E. P. (1999). Airborne laser scanning: existing systems and firms and other resources. *ISPRS J. Photo. Rem. Sens.*, **54**(2-3), 164-198.

Blair, J.B., D.L. Rabine, and M.A. Hofton (1999). The Laser Vegetation Imaging Sensor: a medium-altitude, digitisation-only, airborne laser altimeter for mapping vegetation and topography. *ISPRS J. Photo. Rem. Sens.*, **54**(2-3), 115-122.

Bufton, J.L., and J.B. Blair (1996). Space Laser Altimetry: laser engineering for multiple-beam applications. *Rev. Laser Eng.*, 2**4**, 1285-1292.

Chappelle, E.W., F.M.. Wood, J.E. McMurtrey, and W.W. Newcomb (1984). Laser induced fluorescence of green plants 1. A technique for the remote detection of plant stress and species determination. *Appl. Optics,* **23,** 134-138.

Chappelle, E.W., M.S. Kim, C.L. Mulchi, C.S.T. Daughtry, J. McMurtrey, and L. Corp (1999). Laser Induced Fluorescence (LIF) as a remote sensing tool. A REVIEW. *IEEE Geoscience and Remote Sensing Society Newsletter*, **110,** 6-15.

Dubayah, R., J.B. Blair, J.L. Bufton, D.B. Clark, J. Jala, R. Knox, S.B. Luthke, S. Prince, and J. Weishampel (1997). The Vegetation Canopy Lidar mission. *Proc. Conf. Land Satellite Information in the Next Decade II. American Society for Photogrammetry and Remote Sensing,* 100-112.

Lefsky, M.A., D. Harding, W.B. Cohen, G. Parker and H.H. Shugart (1999). Surface lidar remote sensing of basal area and biomass in deciduous forests of Eastern Maryland, USA. *Remote Sens. Environ.*, **67**, 83-98.

Ludecker, W., H.-G. Dahn, K.P. Gunther and H. Schultz (1999). Laser-Induced Fluorescence-A method to detect the vitality of Scots Pines. *Remote Sens. Environ.*, **68**, 225-236.

Maclean, G.A., and W. Krabill (1986). Gross-merchantable timber volume estimation using an airborne lidar system. *Can. J. Remote Sens.,* **12**, 7-18.

Means, J.E., S. Acker, D.L. Harding, J.B. Blair, M.A. Lefsky, W.B. Cohen, M.E. Harmon, and W.A. McKee (1999). Use of a large-footprint scanning airborne lidar to estimate forest stand characteristics in the Western Cascades of Oregon. *Remote Sens. Environ.*, **67**, 298-308.

Nelson, R., W. Krabill, and G. Maclean (1984). Determining forest canopy characteristics using airborne laser data. *Remote Sens. Environ.*, 15, 201-212.

Nilsson, M., (1996). Estimation of tree heights and stand volume using an airborne lidar system. *Remote Sens. Environ.*, **56**, 1-7.

Standards Australia / Standards New Zealand (1997). Laser safety. Part 1: Equipment classification, requirements and user's guide. 111p. AS/NZS 2211.1:1997.

Standards Australia / Standards New Zealand (1999). Laser safety. Part 1: Equipment classification, requirements and user's guide. Supplement 1: Application guidelines and explanatory notes. 36p. AS/NZS 2211.1:1997. Supp 1:1999.

Appendix 1: The hybrid data acquisition system

The acquisition system used to acquire data from the TDS380 digital oscilloscope is depicted below. The hybrid system was necessary because the TDS380 was not compatible with the existing lidar acquisition system and could not transfer data rapidly enough to the computer. Signals from the detectors were directed via 50-ohm loads to the TSD380. The photodiode sensed the laser output pulse and provided a direct trigger for the RTD710A digitiser and an indirect trigger for the TDS380 and EOC computer (PC-EOC) via a pulse counter / divider circuit. The photodiode signal could also be recorded on the TDS380 by replacing the signal from the second PMT detector with the photodiode output. The EOC PC recorded all the analogue signals and the lidar control and acquisition computer recorded all the digital housekeeping information. Time stamps on the corresponding files recorded to 0.1 seconds resolution are used to match the signal data and housekeeping information recorded on the different computers.
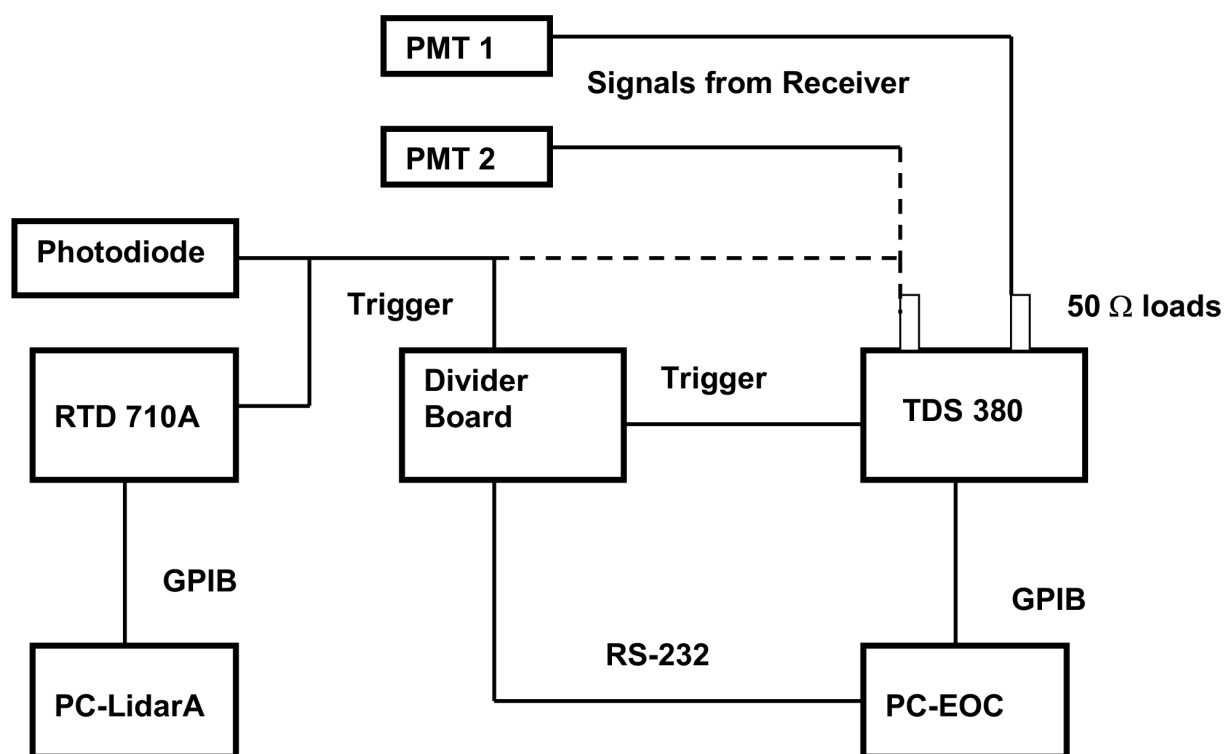
CSIRO Atmospheric Research Technical Papers

(Series title changed from CSIRO Division of Atmospheric Research Technical Papers at number 38)

From July 2000, all new Technical Papers will appear on our Web site; some of these Technical Papers may also appear in paper form.

No. 1 Galbally, I.E.; Roy, C.R.; O'Brien, R.S.; Ridley, B.A.; Hastie, D.R.; Evans, W.J.F.; McElroy, C.T.; Kerr, J.B.; Hyson, P.; Knight, W.; Laby, J.E.
Measurements of trace composition of the Austral stratosphere: chemical and meteorological data. 1983. 31 p.

No. 2 Enting, I.G.
Error analysis for parameter estimates from constrained inversion. 1983. 18 p.

No. 3 Enting, I.G.; Pearman, G.I.
Refinements to a one-dimensional carbon cycle model. 1983. 35 p.

No. 4 Francey, R.J.; Barbetti, M.; Bird, T.; Beardsmore, D.; Coupland, W.; Dolezal, J.E.; Farquhar, G.D.; Flynn, R.G.; Fraser, P.J.; Gifford, R.M.; Goodman, H.S.; Kunda, B.; McPhail, S.; Nanson, G.; Pearman, G.I.; Richards, N.G.; Sharkey, T.D.; Temple, R.B.; Weir, B.
Isotopes in tree rings. 1984. 86 p.

No. 5 Enting, I.G.
Techniques for determining surface sources from surface observations of atmospheric constituents. 1984. 30 p.

No. 6 Beardsmore, D.J.; Pearman, G.I.; O'Brien, R.C.
The CSIRO (Australia) Atmospheric Carbon Dioxide Monitoring Program: surface data. 1984. 115 p.

No. 7 Scott, J.C.
High speed magnetic tape interface for a microcomputer. 1984. 17 p.

No. 8 Galbally, I.E.; Roy, C.R.; Elsworth, C.M.; Rabich, H.A.H.
The measurement of nitrogen oxide (NO, NO2) exchange over plant/soil surfaces. 1985. 23 p.

No. 9 Enting, I.G.
A strategy for calibrating atmospheric transport models. 1985. 25 p.

No. 10 O'Brien, D.M.
TOVPIX: software for extraction and calibration of TOVS data from the high resolution picture transmission from TIROS-N satellites. 1985. 41 p.

No. 11 Enting, I.G.; Mansbridge, J.V.
Description of a two-dimensional atmospheric transport model. 1986. 22 p.

No. 12 Everett, J.R.; O'Brien, D.M.; Davis, T.J.
A report on experiments to measure average fibre diameters by optical fourier analysis. 1986. 22 p.

No. 13 Enting, I.G.
A signal processing approach to analysing background atmospheric constituent data. 1986. 21 p.

No. 14 Enting, I.G.; Mansbridge, J.V.
Preliminary studies with a two- dimensional model using transport fields derived from a GCM. 1987. 47 p.

No. 15   O'Brien, D.M.; Mitchell, R.M.
Technical assessment of the joint CSIRO/Bureau of Meteorology proposal for a geostationary imager/ sounder over the Australian region. 1987. 53 p.

No. 16   Galbally, I.E.; Manins, P.C.; Ripari, L.; Bateup, R.
A numerical model of the late (ascending) stage of a nuclear fireball. 1987. 89 p.

No. 17   Durre, A.M.; Beer, T.
Wind information prediction study: Annaburroo meteorological data analysis. 1989. 30 p. + diskette.

No. 18   Mansbridge, J.V.; Enting, I.G.
Sensitivity studies in a two- dimensional atmospheric transport model. 1989. 33 p.

No. 19   O'Brien, D.M.; Mitchell, R.M.
Zones of feasibility for retrieval of surface pressure from observations of absorption in the A band of oxygen. 1989. 12 p.

No. 20   Evans, J.L.
Envisaged impacts of enhanced greenhouse warming on tropical cyclones in the Australian region. 1990. 31 p. [Out of print]

No. 21   Whetton, P.H.; Pittock, A.B.
Australian region intercomparison of the results of some general circulation models used in enhanced greenhouse experiments. 1991. 73 p. [Out of print]

No. 22   Enting, I.G.
Calculating future atmospheric CO2 concentrations. 1991. 32 p.

No. 23   Kowalczyk, E.A.; Garratt, J.R.; Krummel, P.B.
A soil-canopy scheme for use in a numerical model of the atmosphere — 1D stand- alone model. 1992. 56 p.

No. 24   Physick, W.L.; Noonan, J.A.; McGregor, J.L.; Hurley, P.J.; Abbs, D.J.; Manins, P.C.
LADM: A Lagrangian Atmospheric Dispersion Model. 1994. 137 p.

No. 25   Enting, I.G.
Constraining the atmospheric carbon budget: a preliminary assessment. 1992. 28 p.

No. 26   McGregor, J.L.; Gordon, H.B.; Watterson, I.G.; Dix, M.R.; Rotstayn, L.D.
The CSIRO 9-level atmospheric general circulation model. 1993. 89 p.

No. 27   Enting, I.G.; Lassey, K.R.
Projections of future CO2. with appendix by R.A. Houghton. 1993. 42 p.

No. 28   [Not published]

No. 29   Enting, I.G.; Trudinger, C.M.; Francey, R.J.; Granek, H.
Synthesis inversion of atmospheric CO2 using the GISS tracer transport model. 1993. 44 p.

No. 30   O'Brien, D.M.
Radiation fluxes and cloud amounts predicted by the CSIRO nine level GCM and observed by ERBE and ISCCP. 1993. 37 p.

No. 31   Enting, I.G.; Wigley, T.M.L.; Heimann, M.
Future emissions and concentrations of carbon dioxide: key ocean/atmosphere/land analyses. 1994. 120 p.

No. 32   Kowalczyk, E.A.; Garratt, J.R.; Krummel, P.B.
Implementation of a soil-canopy scheme into the CSIRO GCM — regional aspects of the model response. 1994. 59 p.

No. 33   Prata, A.J.
Validation data for land surface temperature determination from satellites. 1994. 40 p.

No. 34   Dilley, A.C.; Elsum, C.C.
Improved AVHRR data navigation using automated land feature recognition to correct a satellite orbital model. 1994. 22 p.

No. 35   Hill, R.H.; Long, A.B.
The CSIRO dual-frequency microwave radiometer. 1995. 16 p.

No. 36   Rayner, P.J.; Law, R.M.
A comparison of modelled responses to prescribed CO_2 sources. 1995. 84 p.

No. 37   Hennessy, K.J.
CSIRO Climate change output. 1998. 23 p.

No. 38   Enting, I. G.
Attribution of greenhouse gas emissions, concentrations and radiative forcing. 1998. 29 p.

No. 39   O'Brien, D.M.; Tregoning, P..
Geographical distributions of occultations of GPS satellites viewed from a low earth orbiting satellite. 1998. 23 p.

No. 40   Enting, I.G.
Characterising the temporal variability of the global carbon cycle. 1999. 23 p.

No. 42   Mitchell, R.M.
Calibration status of the NOAA AVHRR solar reflectance channels: CalWatch revision 1. 1999. 20 p.

No. 43   Hurley, P.J.
The Air Pollution Model (TAPM) Version 1: technical description and examples. 1999. 41 p.

No. 44   Frederiksen, J.S.; Dix, M.R.; Davies, A.G.
A new eddy diffusion parameterisation for the CSIRO GCM. 2000. 31 p.